Engineering simulations of a super-complex cultural heritage building: Ica Cathedral in Peru.

Maria Pia Ciocci[a*], Satyadhrik Sharma[b], Paulo B. Lourenço[a]

[a] ISISE, Department of Civil Engineering, University of Minho, Guimarães, Portugal

[b] UME School, Istituto Universitario di Studi Superiori (IUSS), Pavia, Italy

Correspondence to Maria Pia Ciocci, ISISE, Department of Civil Engineering, University of Minho, Campus de Azurém, Guimarães, Portugal

E-mail: mariapiaciocci@gmail.com; Tel: +351 966553671

Abstract: The Cathedral of Ica, Peru, is one of the four prototype buildings involved in the ongoing Seismic Retrofitting Project, initiative of the Getty Conservation Institute. The complex historical building, which was heavily damaged by earthquakes in 2007 and 2009, can be divided into two substructures: an external masonry envelope and an internal timber frame built by a construction method known as *quincha* technique. This study makes use of the information available in literature and the results obtained from experimental campaigns performed by Pontificia Universidad Católica del Perú and University of Minho. Nonlinear behaviour of masonry is simulated in the numerical models by considering specified compressive and tensile softening behaviour, while isotropic homogeneous and linear behaviour is adopted for modelling timber with appropriate assumptions on the connections. A single representative bay was initially studied by performing linear elastic analysis and verifying the compliance with the various criteria specified by the applicable normative to discuss the actual failure of Ica Cathedral. Afterwards, the structural behaviour of the two substructures composing the Cathedral is evaluated independently. Finally, the interaction of these two substructures is investigated by performing structural analysis on the entire structure of Ica Cathedral. Several structural analysis techniques, including eigenvalue, nonlinear static and dynamic analyses, are performed in order to: (1) evaluate the dominant mode shapes of the structure; (2) validate the

numerical models by reproducing the structural damage observed in-situ; (3) estimate the structural performance; and (4) identify the main failure mechanisms.

Keywords: unreinforced masonry building; *quincha*-adobe system; finite element (FE) modelling; nonlinear analysis; safety assessment.

1 Introduction

Earth has been used in Peru to construct both monumental and vernacular buildings for almost four thousand years. Remarkable examples of these earthen constructions erected in ancient time include the magnificent structures in Caral (2000 BCE), the urban complexes in Huaca del Sol y de la Luna (100-800 CE), Chan-Chan (850-1476 CE) and Tambo Colorado (1476-1534 CE). Since then, these adobe constructions were combined with the use of a traditional indigenous construction technique known as *quincha* [6]. The technique of *quincha*, or *bahareque*, owed its popularity in the Peruvian coast largely due to the arid climate and the limited supplies of clay soils. As suggested by its etymology – the term *quincha* is derived from the Quechua *kencha* that means "to close" – the technique was originally used to construct primitive huts with frames made of branches and trunks of small trees, which were tied together with vegetal fibres and covered with mud [8].

Although *quincha* was used even before the Incas, it was only during the Hispanic Viceroyalty and the early Republic periods (1534-1821 CE) that it reached its technological climax. Its modest weight and its performance during the earthquakes that occurred in the 17th century in Peru contributed immensely to the wide diffusion of the *quincha* technique for a variety of uses. In 1687, the use of *quincha* technique was ordered by the Spaniards for construction of any building composed by more than one story in Lima: adobe walls were constructed at the ground floor, while the walls of the upper stories, partitions and roofs were built using coarse wood, reeds, mud mats, and clay. Ecclesiastic and other representative buildings, initially erected by the Spaniards with vaults made of brick and stone, were constructed with an external masonry envelope surrounding a complex *quincha* vaulted roofing system. The latter was often composed of several small timber members, assembled together to provide longer spans, which were connected to each other by means of various timber joints and covered by canes, mud layers and lime plasters. Although the construction of these wooden frames was likely to be inspired by the European models, such as those illustrated by Philibert De l' Orme [33], there were significant differences in construction

characteristics and the structural roles of the several structural elements: as an example, while European timber vaulted roofing systems were supported by masonry walls, those constructed in Peru were mainly carried by internal hollow pillars, also built by applying the *quincha* technique [17]. The Church of San Francisco constructed by Constantino de Vasconcelos and Manuel de Escobar (1657-1674) represents the first notable application of the *quincha* technique to construct ecclesiastical buildings, which eventually became the universally adopted solution to rebuild damaged churches and to construct new ones [20, 33].

After Peruvian independence in 1821, these constructions continued to be built throughout the country owing to the easy availability of materials and limited costs involved. It was only after the destructive earthquakes that occurred in Peru in 1868 and in 1908 that the state banned the use of adobe and *quincha* for urban housing and recommended constructions in brick, masonry and reinforced concrete. However, these constructions continued to be still very much in use in the rural areas and they still form a large percentage of the total number of Peruvian buildings [6].

Today, these Peruvian historical structures possess a great value for the society as they represent unique products of the technology of their time and place. Unfortunately, they are at high risk of being irrevocably lost and damaged because of several reasons. Unreinforced masonry structures (URM), especially churches, are typically not designed to withstand horizontal loads [9, 24]. Earthquakes unsurprisingly pose a major threat, especially considering that Peru is situated in one of the most active seismic areas of the world. In 2007 the Pisco earthquake (8.0 M_W) caused severe damage to 58,581 houses [6]. In the Pisco area alone, nearly 80% of the adobe buildings were severely damaged and destroyed by the earthquake; in Ica, 32% of the historical and cultural monuments completely collapsed and 23% were affected by a high degree of damage [5].

The structural performance of URM structures is significantly influenced by several factors: the material properties of masonry (high specific mass, low tensile and shear strengths, and brittle behaviour); the geometry; the mass and stiffness distribution; and the connections between structural elements [21]. Under seismic action, URM structures buildings dissipate energy with the

propagation of damage that leads to the formation of isolated parts that suddenly collapse [2]. On the other hand, timber frames constructed by applying the *quincha* technique show a relatively high tensile strength, exhibiting mostly cracks on the surface of the covering layers. Their collapse is usually due to insufficient structural performance and significant state of decay of the timber connections, and buckling of timber elements [6]. The combination of earth masonry and *quincha* techniques used for these constructions adds even more complexity at any attempt to characterise their global response.

Declared as a national monument since 1982, the Cathedral of Ica was selected by the Getty Conservation Institute (GCI) for the Seismic Retrofitting Project (SRP) as being representative of ecclesial buildings in coastal cities during the Viceroyalty of Peru. Using the Cathedral of Ica as a case study, this paper aims to present a methodology – including data acquisition, structural analysis, diagnosis and safety evaluation – that can be used to carry out safety assessment and to develop effective retrofit methods, if needed, for similar constructions.

2 Relevant seismic events

Since its construction in the 18th century, the cathedral has been subject to a number of seismic events to which its main historical damage can be easily attributed (**Table 1**): the 1813 earthquake (7.5 M_W) provoked the collapse of the front façade, severe damage was caused by the 1868 Arica earthquake (9.0 M_W) and the northern bell tower collapsed after the 1942 earthquake (8.2 M_W). Despite the damage incurred after these earthquakes being heavy, the cathedral was restored to full activity. However, the cathedral is currently in a state of disuse and dilapidation because of recent seismic events. After the Pisco earthquake (8.0 M_W) in 2007 the cathedral suffered partial collapse of the vaults and the main dome, as well as damage of its adobe walls. A later seismic event in 2009 aggravated the already damaged conditions including the total collapse of the main dome (**Fig. 1**) [7, 37, 40].

The western coast of South America is one of the most active seismic areas of the world due to the moving South American plate over the Nazca plate. The Peruvian Building Code divides the entire country into four regions, assigning design peak ground accelerations (PGA) from 0.10g to 0.45g with a probability of exceedance of 10% in 50 years (i.e. corresponding to a return period of 475 years), with Ica being located in the region associated with highest seismic hazard [32]. It should be mentioned that the building code was revised within the duration of this project and the design PGA associated with the location of Ica when the analyses were performed was 0.40g [31].

3 Structural description

A deep insight, into the main features responsible for the intrinsic complexity that characterises the structure of Ica Cathedral along with the numerous unknowns on morphology, was necessary before delving into any form of simulations on such a structure. Such information was primarily derived from information available in literature [7] and additional knowledge derived from an experimental campaign carried out by the University of Minho in May 2015 [18].

The cathedral is located at the corner of an urban block in the historic centre of Ica, over compacted silty sand with little potential for soil liquefaction [26]. It is adjacent to a cloister to the south, while a three-story modern concrete structure is located towards its western side. The cloister was also much damaged in the recent seismic events and has been subsequently repaired. As observed in-situ, the cloister is directly connected at its roof level with the cathedral; for this reason, its buttressing effect was taken into account in the numerical models, as presented in the following sections. The modern reinforced concrete building is fully separated from the cathedral and was ignored subsequently.

The one story cathedral has a rectangular plan oriented along the typical east-west axis. The total plan area of 22.5 x 48.5 m^2 is divided into different functional spaces (**Fig. 2**): a main entrance covered by a choir loft – so-called *sotacoro* – which is flanked by two lateral extensions; a main nave; two side aisles; a transept; and an altar with two chapels on its lateral sides. At the back of the

cathedral, behind the altar and the chapels, a series of spaces is present, including the sacristy, a reception, an internal court and offices.

From the point of view of structural composition, the system of the cathedral can be divided into two main substructures: an inner *quincha* timber frame and an external masonry envelope. The structural details relevant for the numerical modelling of the timber and masonry substructures are presented in Section 3.1 and Section 3.2, respectively.

3.1 *Quincha* timber substructure

The internal space of the cathedral is divided by a series of pillars and embedded pilasters, which support a system of longitudinal and transversal beams, which in turn carry a complex vaulted roofing system. These timber members, which are connected by means of different types of timber joints, including mortice and tenon, half-lap and nailed connections, are either made of cedar (*Cedrelaodorata*), sapele (*Entandrophagmasp*) or huarango (*Prosopissp*), depending on their function in the structure and in accordance to their mechanical characteristics.

The pillars and the pilasters are composed of numerous posts, which are braced by means of horizontal and diagonal elements to increase their resistance against horizontal forces and buckling. Among them, the pillars that separate the main nave from the side aisles contain a huarango trunk located in their central part. These hollow structures are wrapped with flattened cane reeds (*caña chancada*), which are then attached to battens with nailed leather strips and, traditionally, finished with mud plaster and gypsum. The pillars and the pilasters have a fired brick foundation – it is important to note that the bricks at the base of the pilasters do not interlock with the adjoining brick courses of the piers along the lateral walls composing the masonry envelope (Section 3.2).

The complex vaulted roofing system is composed of a large number of different structural elements. A main umbrella dome covers the crossing, while barrel vaults lie above the main nave, the altar, the chapels and the lateral arms of the transept. In particular, the barrel vaults covering the central nave are characterized by lunettes corresponding to the location of the windows in the upper nave walls. The side aisles are covered by small domes, while the extensions flanking the main

entrance are covered by a rib-vaulted ceiling with a flat roof. All the areas surrounding the aisle domes, and also the space between the timber and the masonry substructures, are covered by a flat wooden ceiling. In general, the domes are composed of ribs and two ring beams located at the top and at the bottom, while the barrel vaults are constructed by a system of principal and secondary arches composed of several timber elements made of nailed planks. *Caña chancada* and cane reeds finished with layers of mud plaster (*caña brava*) cover the intrados and the extrados of the vaulted roofing frame respectively, whereas layers of fired brick masonry and sand, lime and cement mortar cover the flat wooden ceiling.

3.2 Masonry envelope

The exterior massive masonry envelope surrounding the cathedral is composed mainly of the front façade with two bell towers, the lateral walls and the back façade, which is not visible externally. The envelope is constructed over base courses of fired brick as well as rubble stone masonry, both of them using a sand and lime based mortar. The base courses vary significantly in their configuration and dimension throughout the building. The masonry envelope is typically finished with mud plaster and gypsum. However, cement plaster most probably from modern renovation works can be found at several locations, including the external base of the northern lateral wall and the top of the bell towers.

The 21 m long Neoclassical front façade is made of fired brick masonry in lime mortar. Its thickness varies with height, ranging from 2.25 m at its base to approximately 0.60 m at the top. This front façade is connected to the internal timber substructure (*sotacoro*) by means of timber joists embedded 0.10 m in the brick masonry (**Fig. 3a**). The 20 m high bell towers flanking this facade are composed of timber frames made of huarango posts resting on wooden plates embedded in the brickwork of the base. The fired brick bases of the bell towers, each approximately 3.80 x 3.80 m^2 in plan, have cavities accommodating stairwells or storage rooms.

The two lateral walls on either side of the front façade and adjoining the two bell towers are constructed with adobe masonry and mud mortar, having a thickness ranging between 1.0 m and 2.0

m. Their total height is about 6.75 m, including the base courses of fired brick and rubble stone masonry above the ground level. Along these lateral walls, behind each pilaster in the side aisles, a series of adobe piers reinforced with fired brick masonry are present. These piers are connected to the beams of the timber substructure, as shown in **Fig. 3b**, and probably to the posts of the pilasters; however, no quantitative information is available regarding this.

4 Mechanical and material characterization

4.1 Timber

Isotropic homogeneous and linear behaviour was assumed for the timber elements in the numerical models. In accordance to Eurocode 5 [12], the mean values of stiffness were adopted in the structural analysis, also considering that the aim of this work is to carry out the safety assessment of Ica Cathedral. It is important to note that since linear elastic analyses were performed on the representative bay, the verifications presented in Section 5.3 were carried out using the characteristic values of modulus of elasticity and the design load-carrying capacities. Moreover, despite the modelling assumption adopted for timber, it should be clarified that the verifications were carried out adopting different strengths along the different directions.

The density and the mean value of modulus of elasticity for the different wood species present in Ica Cathedral – cedar, sapele, huarango – were assumed in the numerical models on the basis of the results obtained from the experimental campaign carried out by the Universidad Nacional Agraria La Molina (UNALM) in 2012, as presented in **Table 2**. However, it should be mentioned that the density value assigned to many elements in the numerical models was not equal to the value corresponding to the wood species in which the timber element is constructed. In order to take into account the weight of the *quincha* covering layers, an increase in the density value was assumed by calculating an equivalent specific weight assigned to the timber elements carrying them. The equivalent specific weight w_{eq} of these timber elements was obtained by using Eq. 1

$$w_{eq} = \frac{w_t \cdot V_t + w_c \cdot V_c}{V_t} \quad \text{Eq. 1}$$

where: w_t is the specific weight of the timber element calculated according to **Table 2**; w_c is the specific weight of the *quincha* layer covering the timber element assumed as 18 kN/m^3; V_t is the volume of the timber element; V_c is the volume of the covering layer. In particular, the latter was calculated assuming 8.5 cm thick covering layers of the vaulted roofing system, while a thickness of 30 cm was adopted for covering layers of the flat wooden ceiling. It should be mentioned that no increase in stiffness due to the confinement effect of these covering layers was considered and the mean value of the modulus of elasticity assigned to each element in the numerical model was assumed to be equal to the value corresponding to the wood species in which the timber member is constructed.

Admissible load-carrying capacities were assumed for each wood species considering the classification performed by UNALM into the structural wood classes recommended in the Peruvian Code [30], as summarized in **Table 2**. From the admissible strengths R_{adm}, the characteristic load-carrying capacities R_k were derived using Eq. 2 provided in the Peruvian Code [30]:

$$R_k = \frac{FS - FDC}{FC - FT} R_{adm} \quad \text{Eq. 2}$$

Here FS is the safety factor assumed as 2.00; FDC is the factor taking into account the duration of loading assumed as 1.15; FC is the factor taking into account timber defects that was assumed as 0.80; FT is the size factor assumed as 0.90. In turn, the design load-carrying capacities R_d were calculated by applying Eq. 3 [12]:

$$R_d = k_{mod} \cdot \frac{R_k}{\gamma_M} \quad \text{Eq. 3}$$

Here γ_M is the partial safety factor assumed as 1.30 for solid timber and k_{mod} is the modification factor taking into account the duration of load and moisture content that was assumed as 0.60 and 1.10 to carry out the verification for ULS under vertical load (1.35G) and under earthquake load combination (G+E), respectively. Finally, the characteristic values of the modulus of elasticity of

each wood species were assumed as provided in the Peruvian Code [30] for the corresponding structural wood class.

4.2 Masonry

In order to simulate the mechanical behaviour of masonry, the Total Strain Rotating Crack (TSRC) material model that is available in DIANA [38] was used in this study. Based on the Total Strain crack model developed along the lines of the Modified Compression Field Theory of [41] and its 3D extension by [36], it describes the stress as a function of the strain and follows a smeared approach for the fracture energy. The crack directions are updated to rotate with the principal directions during the loading process and the constitutive relations are evaluated in the principal directions of the strain vector. This allows to handle the 3D nature of the problem specifying one stress-strain relationship for the principal directions. The cracking phenomenon for the TSRC constitutive law is quantified by the integral under the stress-strain diagram, denoted as fracture energy G_f^I for tension and G_c for compression (**Fig. 4**). In **Fig. 4**, f_c and f_t denote the compressive and tensile strength of masonry whereas h corresponds to the crack bandwidth, which in this case was regularized to ensure mesh independency. For all typologies of masonry present in the numerical models, tensile stresses were assumed to diminish exponentially, while under compression an initial hardening gave way ultimately to a softening defined by a parabolic curve.

The input material properties of the three different types of masonry present in Ica Cathedral – i.e. adobe, fired brick and rubble stone – were derived from bibliographic resources and national technical building standards, considering also the results of the experimental campaign performed by the Pontificia Universidad Católica del Perú (PUCP) in 2012 [42]. For existing historical masonry constructions, adherence to the requirements of modern building standards in calculation of material parameters is often deemed too conservative and / or impossible. Moreover, the material characterisation presented here is with the intent of performing advanced nonlinear analyses, which is generally not very sensitive to input data if changes in the material properties are reasonable and the failure of the structure is controlled by out-of-plane mechanisms [2]. For these reasons,

unreduced values of strength were used in the numerical models to carry out the safety assessment of this structure.

Compression tests were performed by PUCP on three adobe wallets constructed with adobe units from Ica Cathedral and average values of 0.46 MPa and 98 MPa were obtained for compressive strength and modulus of elasticity, respectively. A mean value of 0.05 MPa was adopted for the tensile strength of adobe masonry, which is very close to lower bound value recommended in Eurocode 6 [13]. It should be mentioned that this value was also very similar to those derived by PUCP from shear compression tests performed on three adobe triplets, which were constructed with adobe blocks extracted from the Ica Cathedral and mortar to which straw had been added.

No tests were carried out on fired brick masonry specimens extracted from Ica Cathedral. However, most fired brick masonry present in the cathedral belong to the 19th century, having been constructed in post-earthquake structural interventions. This makes them contemporary to the fired brick masonry present in Hotel El Comercio, another prototype building from the SRP project, from which fired brick masonry wallets had been extracted and tested by PUCP. The sand-lime based mortar used in both structures had undergone significant deterioration with time, and using the results from the specimens extracted from Hotel El Comercio while characterising the brick masonry in Ica Cathedral, allowed the inclusion of its effect on material strength. Possibly due to the low strength of this decayed mortar, an average compressive strength of 1.70 MPa was calculated after compression tests on five specimens, despite the brick units themselves being in good condition. A significant scatter was observed in the values of modulus of elasticity derived from the experimental campaign, and hence the value of modulus of elasticity E was calculated from the compressive strength f_c by using the following relation:

$$E = \alpha \cdot f_c \qquad \text{Eq. 4}$$

The value of α ranges between 200 and 1000 according to Tomaževič [39] and a value of 550 is suggested in FEMA 306 [16], even though the proposed value in Eurocode 6 is 1000 [13].

Adopting the lower limit of the suggested values, the mean value of modulus of elasticity was assumed as 340 MPa. Shear compression tests were also performed on bricks from Hotel El Comercio but with a new mortar. However, considering the effect of material deterioration on the compressive strength of the same masonry, such test data could not be considered representative of masonry present in the Ica Cathedral. Hence, a mean value of tensile strength of 0.1 MPa was adopted from the range of values proposed in Eurocode 6 [13].

Since no experimental tests were possible to be performed on rubble stone masonry present at the foundation of Ica Cathedral, the mean value of compressive strength was derived from the Italian Technical Building Norm [28] and assumed as 0.60 MPa. Using Eq. 4, the mean value of modulus of elasticity was calculated with a value of 300 MPa. On choosing a value closer to the lower limit of the range values suggested values in Eurocode 6 [13], which is presumably more suitable for traditional rubble stone masonry, the mean value of 0.06 MPa was assumed for the tensile strength.

A summary of the material properties adopted for the different typologies of masonry is presented in **Table 3**. It should be noted that the values of fracture energies were adopted on the basis of information available in literature [2] and the moduli of elasticity were subsequently calibrated by performing a model updating of the masonry envelope, as presented in Section 7.2.

5 The representative bay

5.1 Definition of the numerical model

As an initial step towards understanding the global behaviour of the structure, a 3D finite element (FE) model of a representative bay was first constructed in SAP 2000 software [11]. The model included all the structural parts composing a representative bay: a barrel vault with lunettes; two aisles' domes; a system of longitudinal and transversal beams; two nave pillars and two pilasters. The material properties calculated according to Section 4.1 and the cross-sections of the timber elements used for the model of the representative bay are presented in **Table 4**.

Fig. 5 presents the FE model of the representative bay, composed of 1136 nodes and 1344 *frame* elements. Regarding the boundary conditions, the base of the posts composing the nave pillars and pilasters was pinned. Moreover, suitable restraints were applied in terms of horizontal displacement and rotation, defined by the symmetry of the structure. It should be noted that the representative bay was assumed to be self-supported and no restraint was assumed in correspondence to the connection with the longitudinal masonry walls in this model. However, studies carried out in parallel on the model of the representative bay taking into account the presence of these walls provided negligible difference with the results reported in this section. This is most likely because of the high stiffness of the pillars themselves. Concerning the timber joints in the bay, they were modelled as hinged or continuous connections, depending on their mechanical behaviour. Moreover, some adjustments were necessary in order to simulate a realistic distribution of internal forces, such as torsional release of some connections.

5.2 Parametric analysis

The definition of the connections between the timber elements is one of the primary factors adding complexity to the timber substructure of Ica Cathedral. To evaluate the relative importance of the various joints to the global behaviour of the representative bay, parametric analyses were carried out by applying self-weight and mass proportional lateral load (representative of the seismic action) in the transversal direction.

A comparison between the reference model described in Section 5.1, which is expected to be the best representation of the structure, was carried out with models differing only by the modelling of independent sets of timber joints. In particular, the following four models were constructed (**Fig. 6**): SB-0 with rigid connections for all joints; SB-1 with hinged connection for the joints of the posts with beams, diagonal and horizontal elements; SB-2 with hinged connection for the joints between the vertical ribs of the aisles' domes with the ring beams at the top and the bottom; SB-3 with hinged connection for the joints between the barrel vault and the lunettes. It should be noted

that only the specified set of timber joints was modelled as hinged in the models above. In other words, the models were not additive.

The structural response of the representative bay was investigated in terms of structural stiffness defined as the slope from load-displacement diagrams. In particular, the control node was assumed at the top of the lunette, where the maximum lateral displacement was observed. As shown in **Table 5**, the value of linear elastic stiffness obtained for the model SB-0, with rigid connections, represented the upper bound value of stiffness for the representative bay as $7.7 \cdot 10^3$ kN/m. The timber connections of the posts with beams, diagonal and horizontal elements in model SB-1 provided a linear elastic stiffness value of $6.4 \cdot 10^3$ kN/m, slightly lower than the previous one. On the contrary, a significant decrease in global stiffness ($4.7 \cdot 10^3$ kN/m) was observed when the timber connections between the ribs and the ring beams of the aisles' domes were modelled as hinged in model SB-2. The linear elastic stiffness of the structure decreased drastically to a value of $1.3 \cdot 10^3$ kN/m when the bending moment was released for the nodes representing the set of the timber joints between the elements of the barrel vault with lunettes (model SB-3). The value reached in this model is almost the same of that obtained for the reference model ($1.2 \cdot 10^3$ kN/m).

The results showed that the timber connections of the elements composing the barrel vault with lunettes are the most important to control the largest transversal horizontal displacement, which can be considered as a measure of the lateral stiffness of the representative bay whereas the pillars stiffness are rather insensitive the connections of their timber elements.

5.3 Compliance with Eurocode 5

In order to investigate the capacity of sustaining vertical and horizontal actions, linear elastic analysis was performed on the model of the representative bay considering different load conditions and the compliance with the various criteria specified by the Eurocode 5 [12] was evaluated both for Serviceability Limit State (SLS) and Ultimate Limit State (ULS).

Global verifications were carried out on all the straight elements of the representative bay for SLS under self-weight (G) and live load (Q), and for ULS under vertical load (1.35G). In

particular, a value of 0.50 kN/m^2 was adopted for the live load since access to the roofing system was assumed only for maintenance and inspections. The seismic action E was considered by applying mass proportional lateral loading after having introduced the self-weight load, and the verifications were carried out for ULS under earthquake load combination (G+E).

In accordance with Eurocode 5 [12], the instantaneous deformation and the final deformation were evaluated for SLS. The former was calculated by applying the characteristic load combination to the numerical model, while the latter was obtained for the quasi-permanent one. The verification was carried out considering the recommended limit values for instantaneous and final deflections in Eurocode 5 [12], which are expressed in terms of the length of the timber element to be verified. It should be mentioned that for the symmetrical elements of the structure, including the beams at the top of the lunettes, the full span was considered. For the verifications for SLS, the values of displacement which occurred in the beams at the top of the lunettes and those close to the masonry were slightly higher than those recommended. However, existing historical timber structures often show high values of deformation without affecting significantly their usage.

As regards the verifications for ULS, the combination of all the stresses was considered for each of the structural elements, given the three-dimensional nature of the problem, and in turn actions were compared to the design load-carrying capacities. Under vertical load (1.35G), the verifications were satisfied for all the timber members. On the contrary, the beams at the top of the lunettes were not verified under earthquake load combination (G+E).

In addition to global verifications, local verifications were performed for the connections, as recommended in Eurocode 5 [12]. Thought to be the main reason of the collapse of the roofing system of Ica Cathedral during the 2007 Pisco earthquake, and identified as critical joints by the parametric analyses, the mortise and tenon connections of the beams at the top of the lunettes were verified for ULS (**Fig. 7**). These verifications were carried out for the tenons considering the internal forces occurring in the secondary arches and the lunettes' ribs (T1, T2 and T3), and for the cross-sections with mortise considering the internal forces occurring in the beams at the top of the

lunette (M1, M2 and M3), as presented in **Fig. 7**. As regards the beams at the top of the lunettes, these were mainly subjected to biaxial shear and bending moments. Considering the cross-section of the beam with the mortise, the maximum bending stress σ_{max} was calculated by applying Navier's equation (Eq. 5), while the maximum tangential stress τ_{max} was obtained by applying Jourawsky's equation (Eq. 6):

$$\sigma_{max} = \sigma_{max2} + \sigma_{max3} = \frac{M_2}{W_2} + \frac{M_3}{W_3} \leq f_{m,d} \qquad \text{Eq. 5}$$

$$\tau_{max} = \sqrt{\left(\tau_{21}(V_2) + \tau_{21}(V_3)\right)^2 + \left(\tau_{31}(V_2) + \tau_{31}(V_3)\right)^2} \leq f_{v,d} \qquad \text{Eq. 6}$$

Here, the subscripts 1, 2 and 3 indicate the local axes of the *frame* element, 1 being the longitudinal direction and 2, 3 the directions along the cross-section width and height, respectively; $f_{m,d}$ is the design bending strength; $f_{v,d}$ is the design shear strength; M_i, W_i and V_i are the bending moment, the section modulus and shear force corresponding to axis i. Regarding the tenons, compressive axial force and biaxial shear occurred in the secondary arches and the lunettes' ribs. The compressive stress σ was calculated as the ratio between the axial force P and the contact area between the elements, while the tangential stress τ was obtained by applying Eq. (5). Under vertical load (1.5G) the verifications were satisfied for all the cross-sections with mortise of the beams at the top of the lunettes and for the tenons. On the other hand, the stresses that occurred in the cross-sections with mortise of the beams at the top of the lunette under earthquake load combination (G+E) were calculated as large enough to provoke the failure of the structure.

The global and local verifications performed on the representative bay validated the primary causes behind the damage observed for the timber structure of Ica Cathedral after the recent earthquakes, i.e. the failure of timber connections and the deformation of the structural system by the rocking motion (**Fig. 8**). Moreover, these results also shed new light on the reason for which the roofing system of Ica Cathedral did not collapse totally, a phenomenon which was observed in similar constructions, such as the Church of Guadalupe in Ica. In these structures, the *quincha* barrel vaults (without lunettes) restrained the rocking of the walls and high values of stresses were reached

in the connection with the masonry until its failure [6]. Contrary to this, in Ica Cathedral, the failure of the beams at the top of the lunettes partially prevented the onset of this mechanism and only the central part of the barrel vaults collapsed.

6 *Quincha* timber substructure

6.1 Definition of the numerical model

A 3D FE model of the whole timber substructure was created in Midas FX+ Version 3.3.0 Customized Pre/Post processor for DIANA software [38], including all the structural parts presented in Section 3.1. Regarding the *quincha* roofing system covering the main entrance, the transept, the chapels and the altar, similarities were assumed with the representative bay, given the limited information available. More details can be found in [22].

Class–I beams two-noded elements, which take into account shear deformation, were used for the elements of this model. In total, the FE mesh consisted of 17,209 elements and 15,083 nodes. Translational displacements were restrained at the base of posts composing the nave pillars and of the pilasters, and in correspondence to the connection with the masonry walls. The timber joints were modelled as rigid connections, given the need to simplify the model.

6.2 Linear elastic analysis

The structural behaviour of the complex timber substructure was qualitatively studied in terms of linear elastic analysis under self-weight, mass proportional lateral loading and eigenvalue analysis. Under self-weight, high displacements were observed for the transept and the barrel vault covering the altar, with a maximum value of 1.8 cm (**Fig. 9**). It should be mentioned that the displacement that was observed in the longitudinal beams close to the masonry walls was 5.0 mm, approximately. Compared to the results obtained from the analysis of the representative bay, this value is almost four times lower – this is expected considering the assumption regarding the rigidity of timber joints in the model. In terms of internal forces, the ribs composing the main dome showed relatively low values of compressive axial force, while the ring beam at its bottom was subjected to

significant combined internal forces. Moreover, high compressive axial forces with biaxial bending moments were observed in the posts of the central pillars supporting the structure. On the whole, the crossing of the transept was identified as the most critical part, as also confirmed by the results obtained from the eigenvalue analysis. **Fig. 10** shows the mode shapes with the modal participation mass percentage higher than 20% which identified the main dome, as well as the central part of the barrel vault with lunettes, as the most likely vulnerable regions of the structure. Under a mass proportional lateral load applied in the XX (or longitudinal) and YY (transversal) directions, the largest displacements were concentrated in the upper part of the structure: in the main dome as well as in the barrel vaults, which are the relatively less stiff parts of the structure. At the level of the pillars, which is the relevant part for an integrated timber / masonry envelope analysis, similar displacements are found in both models.

Given the simplified assumptions regarding the stiffness of timber connections in this model, the obtained results provided only a qualitative distribution of displacements and stresses. Nevertheless, these results coupled with the in-depth analysis of the representative bay help in understanding several key characteristics of the response exhibited by this complicated timber substructure. In fact, the model of the timber substructure represented an important stepping stone that was necessary for a gradual and controlled increase in complexity from the FE model of the masonry envelope to the one considering both the substructures presented.

7 Masonry substructure

7.1 Definition of the numerical model

A 3D FE model of the masonry substructure was constructed in Midas FX+ Version 3.3.0 Customized Pre/Post processor for DIANA software [38]. The model of the masonry envelope included all the relevant parts of the masonry envelope described in Section 3.2. Huarango lintels, each having a thickness of 30 cm and a bearing of 50 cm into the walls, were inserted at all the

openings of the structure to avoid damage concentrations in the numerical model, which could not be observed in the real structure.

3D isoparametric solid linear four-noded elements were used to model the masonry substructure as well as the bell towers with an average mesh size of 30 cm. The effect of the cloister adjacent to the building was included in the numerical model by using one-noded *translation spring dashpot* elements along the entire length of the southern lateral wall. The stiffness assigned to these springs was calculated to account for the buttressing effect of the columns as well as the roof of the cloister. The created FE mesh of the model of the masonry envelope was composed of 353,866 *3D isoparametric solid linear* elements and 345 *translation spring dashpot* elements, with 81,236 nodes in total. As regards the boundary conditions, all nodes were fixed at the foundation, as normally assumed in structural design – however, this is not very relevant, as cracking could freely occur should the tensile strength be reached. Full connectivity was assumed between intersecting walls, different horizontal layers of masonry and elements composing the bell towers.

7.2 Eigenvalue analysis and model updating

Eigenvalue analysis was first carried out on the numerical model in order to evaluate the dynamic response in terms of natural frequencies and mode shapes. These results were subsequently compared to those obtained from the dynamic identification tests performed by the University of Minho to allow model updating [18].

Output-only, or ambient vibration, tests were performed with measurements during service conditions to define the modal parameters of the structure – natural frequencies, mode shapes and modal damping coefficient – and to calibrate the numerical model. Four piezoelectric accelerometers, having a sensitivity of 10V/g and a frequency range of 0.15 to 1000 Hz (measurement range ±0.5g), were located at the top of the lateral walls considering four different setups. The results were processed using ARTeMIS software [3] by applying both frequency and time domain methods, specifically the Enhanced Frequency Decomposition Domain Method

(EFDD) and the Stochastic Subspace Identification Method (SSI). Since more accurate results were provided by the latter method, only the results obtained by using SSI are presented in this paper.

The test results were used to estimate the first three modes of vibration of the structure as the lowest modes normally have the most significant contribution to the dynamic behaviour of the structure [10]. The value of damping ratio for these modes of vibration ranges between 1.8% and 2.3% with an average value of 2.1%. It should be mentioned that low values of damping ratio are commonly obtained when output-only techniques are used for dynamic identification tests [29]. Moreover, the damping ratio is a sensitive parameter that is difficult to estimate experimentally for historical masonry structures [25]. **Fig. 11** presents the mode shapes obtained from the dynamic identification tests: mode 1 corresponds to the first mode involving the lateral walls with higher intensity of movement observed in the northern wall near the transept area; mode 2 corresponds to a second order curvature of the northern wall, with a deflection point near the middle span; mode 3 identifies a complex mode including the first movement of the façade.

The mode shapes obtained experimentally were compared to those calculated numerically from the FE model of the masonry envelope. As the average error calculated between the frequencies obtained experimentally and numerically for these modes was about 39%, model updating was carried out on the numerical model of the masonry envelope. This was performed by adjusting the values of modulus of elasticity of the different types of masonry in the numerical model within a reasonable range of values in order to match the natural frequencies obtained from the experimental investigations. The average error between the experimental frequencies and those observed for the calibrated model consequently came down to a value lower than 6%. As previously mentioned, the values of the modulus of elasticity of the different types of masonry in the calibrated model are shown in **Table 3**.

It should be mentioned that the first mode obtained experimentally displayed partly in phase movement of both the lateral walls, while movement of significant intensity was observed in only one wall for the corresponding mode used in model updating. This was one of many reasons for

gravitating towards a combined model considering both substructures together. For eigenvalue analysis performed on the combined model, the lateral walls got activated simultaneously in the obtained modes of vibration due to the presence of the timber substructure, providing better correlation between numerical and observed dynamic response.

7.3 Nonlinear analysis

In order to evaluate the seismic behaviour of the masonry envelope only, nonlinear static (pushover) analyses were performed on the calibrated model by applying a mass proportional approach, after having applied the self-weight.

The results obtained from the nonlinear analysis under self-weight showed negligible values of displacements that were in the order of millimetres. The highest value of minimum and maximum principal stresses were calculated to be 0.36 MPa and 0.03 MPa, respectively – both lower than the values of strength assumed for masonry (**Table 3**). Hence, no cracking was observed throughout the masonry envelope, indicating that there was no onset of damage in the masonry under self-weight.

Consequently, the lateral load was applied in the primary axes of the numerical model, in both positive and negative directions. Arc-length method was implemented in these analyses over all the nodes of the FE model to better capture the nonlinear response of the structure [38]. The lateral load-carrying capacity was assessed from load-displacement curves obtained assuming the nodes exhibiting high displacement in the direction of the applied load as control points. For the analyses in the XX- and XX+ directions this control node was chosen to be the top of the pediment of the front façade and the back wall of the sacristy, respectively. For both the analyses in the YY direction, the control node was the top of the wall in the north western corner of the cathedral.

As shown in (**Fig. 12**), the lateral load-carrying capacity was calculated as 0.27g and 0.36g in the XX+ and XX– (longitudinal) directions, respectively. On the other hand, the maximum lateral load that could be applied to the model in the YY+ and YY– (transversal) directions was 0.25g and 0.22g, respectively. It is worth noting that the comparison between the results obtained from the

pushover analyses performed on the calibrated (ME – C) – i.e. with material properties updated in accordance to model updating – and un-calibrated (ME – UC) models showed a moderate increase in lateral load-carrying capacity for the former (around 10%).

The most relevant failure mechanisms of the model of the masonry envelope were identified when lateral load was applied in the XX– and YY– directions, considering the absence of any adjoining structures in these directions. Under the lateral load of 0.36g in the XX– direction, the failure mechanism consisted of the out-of-plane mechanism of both the front façade and the bell towers. When the lateral load of 0.22g was applied in the YY– direction, the failure mechanism was identified as the out-of-plane mechanism of the northern lateral wall – especially of the north-western corner of the structure. Good correlation was observed between the crack pattern obtained from these pushover analyses on the calibrated model and the existing damage observed in-situ, validating the numerical model [22]. It should be mentioned that dynamic nonlinear (time-history) analysis was also performed on the calibrated model of the masonry envelope – applying the methodology applied for the combined model in Section 8.3 – and the obtained results confirmed those obtained from the pushover analyses.

8 Complete structure

8.1 Definition of the numerical model

Based on the geometrical and modelling hypotheses assumed for the numerical models presented in Section 6 and Section 7, a 3D FE model of the entire structure was constructed in Midas FX+ Version 3.3.0 Customized Pre/Post processor for DIANA software [38] in order to investigate the interaction between the two substructures and its effect on the global response of Ica Cathedral. **Fig. 13** shows the FE mesh of the combined model, with 96,340 nodes in total.

The definition of the connections existing between the two structural systems, for which little information was available, represented an important aspect for the construction of this numerical model. The connections between the two substructures were assumed to exist between:

(1) the wooden beams in the upper part of the main entrance and the fired brick façade and the lateral masonry walls; (2) the wooden beams supporting the barrel vaults of the chapels and altar and the masonry walls; and (3) the transversal wooden beams of the bays and the lateral masonry walls. These connections were modelled by merging the nodes of *class–I beam* elements with those of 3D *isoparametric solid linear* elements, and suitable restraints were applied to these nodes in order to avoid compatibility problems.

8.2 Nonlinear static analysis

Nonlinear static analyses were carried out in order to investigate the capacity of the whole structure to support self-weight and lateral loading. The seismic behaviour of the entire structure was evaluated by performing mass proportional lateral loading analyses in the two directions where the most critical failure mechanisms were identified in the model of the masonry envelope – i.e. the XX– and YY– directions.

Fig. 14 shows the results obtained for the combined model under gravity loading. A maximum displacement of 2.0 cm was calculated in the upper part of the barrel vault covering the altar. Significant displacements were also seen in the vaulted roof framing system covering the transept, the chapels and the main nave with values ranging between 1.0 to 1.5 cm. Outwards displacements, with a maximum value of 8.0 mm, were present in both the lateral walls due to the thrust of the timber structure covering the transept and the chapels (**Fig. 14a**). A maximum value of compressive stress was calculated as 0.45 MPa, lower than the compressive strength calculated for all the types of masonry present in the model (**Fig. 14b**). While no tensile damage was observed for rubble stone and fired brick masonries, some concentration of tensile cracking occurred at the location of the connections between the timber structure with the adobe masonry walls. However, the tensile strains were very low compared to the corresponding yielding strain and negligible crack widths were observed. It should be noted that the mesh representing the timber substructure is hidden here for clarity of the results (**Fig. 14c**).

Regarding the pushover analysis in the XX– direction, the maximum lateral load-carrying capacity obtained was 0.45g, the failure mechanism in the masonry envelope being identified as the out-of-plane failure of both the front façade and the bell towers. **Fig. 15a** shows the distribution of displacements of the model when it reached its maximum lateral load-carrying capacity. The highest displacements throughout the masonry envelope were observed in the bell towers, due to the rotation at the base, with a value of about 17.0 cm at peak. Moreover, significant deformation also occurred in the front façade and the walls surrounding the altar. The crack pattern shows tensile damage progressing from the connection between the northern bell tower and the front facade through the base of the former with a maximum crack width of 2.0 cm (**Fig. 15b**). On the other side, vertical separation cracks occurred between the lateral wall and the southern bell tower and diagonal cracks propagated throughout the adobe wall, with an average crack width of 7.0 mm. Moreover, flexural cracks were observed at the base of both the bell towers and the front façade. Extensive tensile damage was also seen where the walls of the altar are connected to other adjoining walls. As the structure entered the post peak behaviour, tensile damage progressed significantly in the façade and the bell towers, those parts of the structure exhibiting independent behaviour with respect to the rest of the structure, as shown in **Fig. 15c**.

When the lateral load was applied in the YY– direction, the maximum lateral load-carrying capacity was calculated to be a value of 0.28g and the failure mechanism consisted of the out-of-plane failure of the northern lateral wall and of the northern bell tower. High values of displacement were observed for these parts under this lateral load, as shown in **Fig. 16a**. In particular, a maximum displacement of 10.5 cm was calculated for the north–western corner of the model at peak. As shown in **Fig. 16b**, extensive vertical cracks were observed in this part with a maximum crack width of 3.5 cm, while a crack width of about 7.0 mm was calculated for the crack separating the southern bell tower from the rest of the structure. Moreover, flexural cracks occurred in the upper part of the adobe wall close to the opening and at the base of the rubble stone base course.

Fig. 16c shows that horizontal cracking between adobe masonry and the fired brick base course was observed in the post peak behaviour, in agreement with damage observed in-situ.

The structural response of the combined model (CM) under lateral loading in the XX– and YY– directions was assessed from load-displacement diagrams. The corresponding capacity curves obtained from the calibrated model of only the masonry envelope (ME – C) are also plotted with them (**Fig. 17**). The results plotted here are calculated at control points assumed at the nodes where high values of displacement were observed: a node at the top of the pediment and one at the top of the north-western corner were considered for plotting the capacity curves of the different models under lateral load in the XX– and YY– directions, respectively. As shown in **Fig. 17**, the combined model presented an increase of about 25% in lateral load-carrying capacity when compared to the model of the masonry envelope, in both the directions. While a similar initial stiffness was observed for ME – C and MC under lateral load in the XX– direction, an appreciable decrease in the initial stiffness was seen for MC as compared to ME – C when lateral load was applied in the other direction. The obtained results pointed out without doubt that the interaction between the two substructures affects significantly the seismic behaviour of the entire structure of Ica Cathedral. Finally, the load-carrying capacities obtained for the combined model were compared to the PGA provided in the Peruvian Code [31], or the ultimate state. As presented in **Fig. 17**, the seismic capacity of even the combined model calculated when the lateral load was applied in the YY– direction was found considerably lower than the PGA (0.45g), further demonstrating the low capacity of the structure when compared to the values required by the code and experienced in the Pisco earthquake.

The safety assessment of this structure in its current state was carried out in this study using a force based method by means of pushover analyses. In this case, the horizontal forces adopted to represent the seismic action were proportional to the mass, independently from their height distribution in the structure, since good correlations have been found in terms of capacity between mass proportional pushover analysis and time history analysis in previous studies performed on

historical constructions [14]. The results obtained from the pushover analyses were used to verify the structural performance by means of verification of base shear and the estimation of failure mechanisms with their damage distribution. The results obtained in terms of base shear were validated by defining, in each step, the ratio of the total horizontal and the total vertical loads of the structure, that is indicated in the pushover curves as "load step". Afterwards, this maximum load step value was compared to the seismic demand that was assumed as the PGA [31]. According to the Italian Code and International Codes, the behaviour factor and the soil factor should be taken into account in order to evaluate the seismic demand; however, a decrease in the PGA is also allowed for existing buildings (2/3 or ¾) [13, 27]. In this study, the authors did not take into account any of these increases/decreases in the seismic demand and they assumed directly the PGA. Finally, it is important to underline that mass proportional analyses activated all the mass of the structure, leading to local failure mechanisms, and low participation mass percentages were observed for fundamental modes in the model.

8.3 Nonlinear dynamic analysis

Time-history analysis was carried out on the combined model to study its dynamic response, to validate it with respect to damage observed in-situ due to past seismic activity and to compare the obtained results with those derived from nonlinear static analyses. Unlikely pushover analyses, nonlinear dynamic analysis can follow the full seismic loading process, considering significant aspects of the structural response, such as the damage produced by reversal of loads and hysteretic behaviour [4]. However, this advanced structural analysis technique is often challenging to perform, not only due the inherent complexity in the method but also the large computational effort involved. Additionally, because of its low tensile strength, masonry responds to dynamic loading with distributed cracks throughout the structure that undergo opening, closing and reopening, a behaviour which is not very easy to control in a nonlinear dynamic analysis [25].

According to Rayleigh formulation $\mathbf{C} = a\mathbf{M} + b\mathbf{K}$, the damping of the structure was simulated in the time-history analysis as a viscous damping considering the classical damping

matrix **C** to be a linear combination of the mass **M** and the stiffness **K** matrices, where a is the mass proportional damping constant and b is the stiffness proportional damping constant [10]. Considering all the natural modes of vibration until 80% mass participation and a damping ratio of 3%, these constants a and b were calculated with a value of 0.3893 and 0.0007876, respectively. The evaluation of damping ratio is rather complex due to the fact that it is related to nonlinear phenomena and is sensitive to the level of vibration [29]. The damping ratio was assumed based on the experience of the authors and [1], noting that the inelastic behaviour introduces additional damping. It should be mentioned that time history analyses of historical masonry structures are typically insensitive to small damping variations [25].

Implicit time step integration using the Hilber-Hughes-Taylor method, also so-called α method [19], was used to perform this analysis, adopting a value for α equal to –0.1 and a time step Δt equal to 0.0045s. In particular, the time step Δt was defined taking into account requirements arising from both the total duration of the analysis (20s) as well as the highest period associated with the modes among those used to calculate the 80% mass participation [38]. It should be mentioned that the use of the α method allows to introduce numerical damping of noise resulting from abrupt changes in masonry from an elastic to fully cracked state with zero stiffness change [15].

The applied seismic input was in the form of two artificial accelerograms generated using SeismoArtif v2.1 [34] and compatible with the elastic response spectrum of the Peruvian Code specified for the region where Ica is located (**Fig. 18**). Additional post-processing of these accelerograms was performed using SeismoSignal v5.1 [35]. In order to apply a single earthquake to the combined model, these artificial accelerograms – which were uncorrelated, i.e. peaks in acceleration do not occur at the same time with respect to each other – were applied to the combined model in two orthogonal directions to each other (XX and YY directions). It is worth to notice that the use of artificial accelerograms could overestimate the response, in comparison with recorded accelerograms, which seem not available.

Fig. 19 shows displacement-time diagrams obtained to study displacements occurring during the time history of loading, The displacement shown in **Fig. 19** denotes the relative out-of-plane displacement calculated for the selected control point with respect to the node at the base directly below it. Similar to the load-displacement diagrams plotted from the results obtained for the pushover analyses, the control points were selected as the node at the top of the pediment and the node at the top of the north-western corner. The maximum value of relative out-of-plane displacement was calculated to be a value of 20.0 cm for the node at the top of the north-western corner, while a value of 14.0 cm was obtained for the node at the top of pediment. These displacements correspond to maximum drift ratios – i.e. the maximum relative out-of-plane displacement divided by the height of the masonry wall – of about 3% and 1.6% respectively, meaning that significant out-of-plane deflection and damage occurred in the model. In fact, it should be mentioned that masonry lost all its load carrying capacity at the end of the applied loading, which was evident also by plotting loading-unloading graphs in both directions of applied loading.

A plot of scan of the maximum principal strains that occurred in the history of the applied loading confirmed this and reflected the severe damage that the model undergone. Critical cracking present in the structure after the earthquakes, such as parallel cracking in the adobe masonry of the northern lateral wall, diagonal cracks in the front façade and separation cracks at the base of the pediment were also reproduced by this analysis confirming the validity of the model. Additionally, damage similar to the failure mechanisms predicted by the pushover analysis was observed in the principal directions in which excitation was applied. It should be mentioned that the nonlinear dynamic analysis also reproduced cracks existing currently in the structure which were not obtained from pushover analyses, where the lateral load was applied monotonically, increased up until the failure and in only one direction (**Fig. 20**, **Fig. 21**).

9 Conclusions

This paper presented the safety assessment of Ica Cathedral, which is composed of two substructures: an external masonry envelope and an inner timber frame constructed by applying the *quincha* technique. This task was challenging due to the complexity of this historical building and to the unknowns on the geometry and material properties. To reach this aim, several numerical models were created based on the information available in literature and experimental campaigns.

A detailed insight into the structural response of a representative bay was an initial step towards understanding the global behaviour of the structure. Parametric analyses were carried out to investigate the effect of the principal timber joints of the representative bay by applying a lateral loading using a mass proportional approach. The obtained results allowed the identification of the most critical timber joints in the representative bay and justification of the damage experience by this substructure. Global and local verifications were carried out in order to evaluate the compliance of the representative bay with the various criteria specified in Eurocode 5. Under vertical loading, the timber members were mostly verified for the SLS and for ULS. When the ULS under seismic combination was considered, the global verifications were not satisfied for the beams at the top of the lunettes, confirming the damage observed in-situ. Moreover, for ULS under earthquake load combination the mortise and tenon connections of the beams at the top of the lunettes were not locally verified, as observed during the earthquake series experienced.

Afterwards, the structural behaviour of the two substructures composing the Cathedral were evaluated independently. According to the qualitative study carried out on the whole timber structure, the posts and the main dome composing the crossing of the transept represent the additional most critical parts, confirming the existing damage. On the other hand, the results obtained from the different pushover analyses performed on the model of the masonry envelope showed that the most relevant failure mechanisms were in the longitudinal (XX–) and transversal (YY–) directions, towards the outside of the building. In particular, the lower bound lateral load-carrying capacity of the masonry envelope was calculated in the YY– direction, with a value of only

0.22g. The north-western corner was identified as the most vulnerable part of the structure, as also confirmed by the results obtained from the time-history analysis.

Although the structural behaviour seems to be reasonably well represented by independent structures, the analyses performed on the combined model of the cathedral demonstrated that the building is influenced by the interaction of the two substructures. Comparing the complete structure with respect to only the masonry envelope, an increase in seismic capacity of about 25% was observed in both directions. The lower bound capacity of the combined model was found in the transversal direction, with a value of 0.28g – much lower than the PGA considered in the code for the region of Ica. Global strengthening is therefore required in order to avoid the out-of-plane mechanisms identified for the most vulnerable regions of the structure. Tying, ring beams and adequate connections between the two substructures can represent efficient strengthening techniques to improve the structural performance of Ica Cathedral.

Acknowledgements

This work was carried out with funding from the Getty Seismic Retrofitting Project under the auspices of the Getty Conservation Institute (GCI). This work is also partially financed by FEDER funds through the Competitivity Factors Operational Programme - COMPETE and by national funds through FCT – Foundation for Science and Technology within the scope of the projects POCI-01-0145-FEDER-007633 and PTDC/ECM-EST/2777/2014.

Disclosure of potential conflicts of interest

The authors declare that they have no conflict of interest.

References

[1] Aguilar R, Marques R, Sovero K, Martel C, Trujillano F, Boroschek R (2015) Investigations on the structural behaviour of archaeological heritage in Peru: From survey to seismic assessment. Eng Struct, 95: 94-111. doi: 10.1016/j.engstruct.2015.03.058

[2] Angelillo M, Lourenço PB, Milani G (2014) Masonry behaviour and modelling. In Angelillo M (ed) Mechanics of Masonry Structures, CISM International Centre for Mechanical Sciences. Springer, Italy, 551: 1-26. doi: 10.1007/978-3-7091-1774-3

[3] ARTeMIS (2014) Modal Users' Manual. SVS - Structural Vibration Solutions A/S. Denmark

[4] Betti M, Galano L, Vignoli A (2015) Time-History Seismic Analysis of Masonry Buildings: A comparison between Two Non-Linear Modelling Approaches. Buildings, 5: 597–621. doi:: 10.3390/buildings5020597

[5] Blondet M, Vargas J, Tarque N (2008) Observed behaviour of earthen structures during the Pisco (Peru) earthquake of August 15, 2007. In Proceedings of the 14th World Conference on Earthquake Engineering, Beijing, China, 12th – 17th October 2008. http://www.iitk.ac.in/nicee/wcee/article/14_01-1031.PDF

[6] Cancino C, Farneth S, Garnier P, Vargas Neumann J, Webster F (2009) Damage Assessment of Historic Earthen Buildings after the August 15, 2007 Pisco, Peru Earthquake. The Getty Conservation Institute, Los Angeles

[7] Cancino C, Lardinois S, D'Ayala D, Ferreira CF, Dávila DT, Meléndez EV, Santamato LV (2012). Seismic Retrofitting Project: Assessment of Prototype Buildings. The Getty Conservation Institute, Los Angeles

[8] Carbajal F, Ruiz G, Schexnayder CJ, ASCE F (2005) Quincha Construction in Peru. Pract Period Struct Des Constr, 10: 56-62. doi: 10.1061/(ASCE)1084-0680

[9] Castellazzi G, Gentilini C, Nobile L (2013) Seismic Vulnerability Assessment of a Historical Church: Limit Analysis and Nonlinear Finite Element Analysis. Adv Civ Eng. doi: 10.1155/2013/517454

[10] Chopra AK (2012) Dynamics of Structures: Theory and Applications to Earthquake Engineering. Prentice Hall, Englewood Cliffs

[11] CSI (2014) Analysis Reference Manual for SAP 2000, ETABS, SAFE and CSiBrisge. Berkeley

[12] EN 1995-1-1 (2004) Eurocode 5: Design of timber structures - Part 1-1: General - Common rules and rules for buildings. CEN, Brussels

[13] EN 1996-1-1 (2005) Eurocode 6: Design of masonry structures – Part 1-1: General rules for reinforced and unreinforced masonry structures". CEN, Brussels

[14] Endo Y, Pelà L, Roca P (2016) Review of Different Pushover Analysis Methods Applied to Masonry Buildings and Comparison with Nonlinear Dynamic. J Earthquake Eng, 1-22. doi: 10.1080/13632469.2016.1210055

[15] Faria R (1994) Seismic Evaluation of Concrete Dams via Continuum Damage Models. PhD Dissertation, University of Minho

[16] FEMA 306 (1998) Evaluation of earthquake damaged concrete and masonry wall buildings - Basic Procedures Manual (ATC-43 Project). ATC – Applied Technology Council, Redwood City

[17] Ferreira CF, D' Ayala D, Fernandez Cabo JL, Diez R (2013) Numerical Modelling of Historic Vaulted Timber Structures. Adv Mat Res, 778: 517–525. doi: 10.4028/www.scientific.net/AMR.778.517

[18] Greco F, Karanikoloudis G, Mendes N, Lourenço PB (2015) Experimental in situ testing campaign on adobe historic structures in Peru, within the Getty SR Project. Report 2015-DEC/E-30. University of Minho – TecMinho, Guimaraes

[19] Hilber HM, Hughes TJR, Taylor RL (1977) Improved numerical dissipation for time integration algorithms in structural dynamics. Earthquake Eng Struct Dynam, 5: 283-292. doi: 1.01002/eqe.4290050306

[20] Hurtado Valdez P (2009) Masonry or Wooden Vaults?: The Technical Discussion to Rebuilt the Vaults of the Cathedral of Lima in the Seventeenth Century. In Kurrer KE, Lorenz W, Wetzk V (eds) Proceedings of the Third International Congress on Construction History, Cottbus, Germany, 20th – 24th May 2009. NEUNPLUS1, Berlin

[21] Lourenço PB, Mendes N, Ramos LF, Oliveira DV (2011) On the Analysis of Masonry Structures without box behaviour. Int J Archit Herit, 5: 369-382. doi: 10.1080/15583058.2010.528824

[22] Lourenço PB, Sharma S, Ciocci MP, Greco F (2015) Seismic Assessment of Ica Cathedral (Current Condition), Peru. Report 2015-DEC/E-34. University of Minho – TecMinho. Guimaraes

[23] Lourenço PB, Trujillo A, Mendes N, Ramos LF (2012) Seismic performance of the St. George of the Latins church: Lessons learned from studying masonry ruins. Eng Struct, 40: 501–518. doi: 10.1016/j.engstruct.2012.03.003

[24] Milani G (2013) Lesson learned after the Emilia-Romagna, Italy, 20–29 May 2012 earthquakes: A limit analysis insight on three masonry churches. Eng Fail Anal, 34: 761-78. doi: 10.1016/j.engfailanal.2013.01.001

[25] Mendes N (2012) Seismic Assessment of Ancient Masonry Buildings: Shaking Table Tests and Numerical Analysis. PhD Dissertation, University of Minho

[26] Mitma M, Grover J, Jorge E, Alva H (2005) Microzonificación de la ciudad de Ica frente a sismos e inundaciones. http://www.cismid.uni.edu.pe/descargas/redacis/redacis27_a.pdf

[27] NTC (2011) Nuove norme tecniche per le costruzioni e circolare esplicativa. Decreto Ministeriale Infrastrutture 14 gennaio 2008 – Circolare 2/02/2009 n°617/C.S.LL.PP. DEI, Roma (in Italian)

[28] OPCM 3431 (2005) Primi elementi in materia di criteri generali per la classificazione sismica del territorio nazionale e di nuove normative tecniche per le costruzioni in zona sismica. Ordinanza P.C.M. n. 3431 del 3 Maggio 2005. Modifica dell'ordinanza n. 3274 del 20 Marzo 2003. Italy (in Italian)

[29] Ramos LF (2007) Damage Identification on Masonry Structures Based on Vibration Signatures. PhD Dissertation, University of Minho

[30] RNE E.010 (2006) Reglamento Nacional de Edificaciones: Norma Técnica E.010 "Madera". Decreto Supremo N° 011-2006-vivienda (05-03-2006). Ministerio de Vivienda, Construcción y Saneamiento, Peru (in Spanish)

[31] RNE E0.30 (2006) Reglamento Nacional de Edificaciones: Norma Técnica E.0.30 "Diseño Sismorresistente". Decreto Supremo N° 011-2006-vivienda (05-03-2006). Ministerio de Vivienda, Construcción y Saneamiento, Peru (in Spanish)

[32] RNE E0.30 (2016) Reglamento Nacional de Edificaciones: Norma Técnica E.030 "Diseño Sismorresistente". Decreto Supremo N° 003-2016-vivienda (24/01/2016). Ministerio de Vivienda, Construcción y Saneamiento, Peru (in Spanish)

[33] Rodríguez Camilloni H (2003) Quincha Architecture: The development of an antiseismic structural system in seventeenth century Lima. In Huerta S (ed) Proceedings of the First International Congress on Construction History, Madrid, 20th-24th January 2003. Instituto Juan de Herrera, Spain, pp 1741-1752

[34] SEiSMOSOFT (2013) Seismoartif v2.1. Pavia

[35] SEiSMOSOFT, (2013) SeismoSignal v5.1. Pavia

[36] Selby RG, Vecchio FJ (1993) Three-dimensional Constitutive Relations for Reinforced Concrete. Tech. Rep. 93-02, University of Toronto

[37] Taucer F, Alarcon J, So E (2009) 2007 August 15 magnitude 7.9 earthquake near the coast of Central Peru: analysis and field mission report. Bull Earthquake Eng, 7 (1): 1-70. doi: 10.1007/s10518-008-9092-3

[38] TNO DIANA (2014) Diana Manuals. http://tnodiana.com/DIANA-manuals

[39] Tomaževič M (1999) Earthquake-Resistant Design of Masonry Buildings. In Tomaževič M (ed) Series on Innovation in Structures and Construction. Imperial College Press, London

[40] USGS (2017) United States Geological Survey, Earthquake Hazards Program. https://earthquake.usgs.gov/. Accessed 10/04/2017

[41] Vecchio FJ, Collins MP (1986) The modified compression field theory for reinforced concrete elements subjected to shear. ACI Journal 83 (22): 219-231. doi: 10.14359/10416

[42] Vicente E, Torrealva DE (2014) Mechanical Properties of Adobe Masonry of Historical Buildings in Peru. In Meli R, Peña F, Cháves M (eds) Proceedings of the 9th International Conference on Structural Analysis of Historical Constructions (SAHC 2014), Mexico City, 14th-17th October 2014.
http://www.hms.civil.uminho.pt/sahc/2014/topic10-fullpaper005.pdf

List of tables

Table 1 Relevant seismic events affecting Ica [7, 37, 40]

Table 2 Material properties of the different types of timber in Ica Cathedral

Table 3 Material properties of the different types of masonry in Ica Cathedral

Table 4 Summary of the properties adopted for a representative bay of Ica Cathedral. Here E_m and w_{eq} are the mean values of the modulus of elasticity and the equivalent specific weight

Table 5 Values of global structural stiffness K obtained from parametric analysis on timber connections of a representative bay

Table 1 Relevant seismic events affecting Ica [7, 37, 40]

Year	Magnitude	Location	Distance epicentre-cathedral site (km)
1813	7.5	Ica, Peru	-
1868	9.0	Arica, Peru (now Chile)	700
1942	8.2	Off the coast of central Peru	130 (approx.)
2007	8.0	Central coast of Peru	110
2009	5.8	Central coast of Peru	200 (approx.)

Table 2 Material properties of the different types of timber in Ica Cathedral

Properties	Huarango	Cedar	Sapele
Density (kg/m^3)	1040	380	490
Mean value of modulus of elasticity in flexure (MPa)	16900	9380	8610
Poisson's ratio (-)	0.30	0.30	0.30
Admissible bending strength (MPa)	20.60	14.70	14.70
Admissible compressive strength parallel to grain (MPa)	14.20	10.80	10.80
Admissible compressive strength perpendicular to grain (MPa)	3.90	2.70	2.70
Admissible tensile strength parallel to grain (MPa)	14.20	10.30	10.30
Admissible shear strength (MPa)	1.50	1.20	1.20
5% value of modulus of elasticity (MPa)	9316	7355	7355
5% value of shear modulus (MPa)	3583	2829	2829

Table 3 Material properties of the different types of masonry in Ica Cathedral

Properties	Adobe	Fired brick	Rubble stone
Specific weight (kN/m^3)	19	19	19
Modulus of elasticity (MPa)	220*	850*	720*
Poisson's ratio (–)	0.20	0.20	0.20
Compressive strength (MPa)	0.46	1.70	1.00
Tensile strength (MPa)	0.05	0.10	0.06
Fracture energy (compression) (N/mm)	1.00	3.50	1.50
Fracture energy (tension) (N/mm)	0.01	0.01	0.01

*Modulus of elasticity obtained from model updating

Table 4 Summary of the properties adopted for a representative bay of Ica Cathedral. Here E_m and w_{eq} are the mean values of the modulus of elasticity and the equivalent specific weight

Structural Part	Element	Wooden Species	w_{eq}(kN/m^3)	E_m(MPa)	Base (m)	Height (m)
Barrel Vault with Lunettes	Principal Arch	Cedar	54.45	9380	0.12	0.25
	Secondary Arch	Cedar	54.45	9380	0.08	0.25
	Beam of the lunette	Sapele	54.45	8610	0.08	0.25
	Diagonal of the lunette	Cedar	54.45	9380	0.08	0.25
	Arch of the lunette	Cedar	54.45	9380	0.12	025
Aisles' Domes	Vertical rib	Cedar	132.73	9380	0.18	0.12
	Ring beam at the top	Cedar	132.73	9380	0.06	0.18
	Ring beam at the bottom	Cedar	132.73	9380	0.06	0.18
Horizontal Elements	Longitudinal beam (I)	Sapele	70.83	8610	0.25	0.12
	Longitudinal beam (II)	Sapele	70.83	8610	0.30	0.12
	Transversal beam (III)	Sapele	70.83	8610	0.25	0.25
	Longitudinal beam (IV)	Sapele	32.35	8610	0.25	0.25
	Deck	Sapele	32.35	8610	0.08	0.12
Frame	Longitudinal frame	Sapele	25.06	8610	0.25	0.12
	Transversal frame	Sapele	39.69	8610	0.25	0.12
Pilaster	Post	Sapele	33.25	8610	0.25	0.12
Nave Pillar	Post (I)	Sapele	27.76	8610	0.25	0.12
	Post (II)	Sapele	27.76	8610	0.25	0.25
	Central post	Huarango	10.20	16900	0.30	0.30
Bracing	Horizontal element	Sapele	4.81	8610	0.10	0.10
	Diagonal element	Sapele	4.81	8610	0.10	0.10

Table 5 Values of global structural stiffness K obtained from parametric analysis on timber connections of a representative bay

	Model SB-0	Model SB-1	Model SB-2	Model SB3	Reference Model
K (kN/m)	$7.7 \cdot 10^3$	$6.4 \cdot 10^3$	$4.7 \cdot 10^3$	$1.3 \cdot 10^3$	$1.2 \cdot 10^3$

List of figures

Fig. 1 Ica Cathedral damage after the earthquakes in 2007 and 2009: **a** front façade, **b** main dome at transept, **c** barrel vaults with lunettes and pillars

Fig. 2 Architectural drawing of Ica Cathedral: **a** ground floor, **b** longitudinal elevation, **c** longitudinal section, **d** front elevation, **e** transversal section (m) [7]

Fig. 3 Connection between the two substructures: **a** front façade/*sotacoro*, **b** piers along the lateral walls/timber beams

Fig. 4 Stress-strain curve showing the Total Strain Rotating Crack material model of masonry adopted in the numerical models [38]

Fig. 5 FE model of the representative bay

Software: SAP 2000

Fig. 6 Set of timber connections for parametric analyses considering hinged connections of elements: **a** model SB-1, **b** model SB-2, **c** model SB-3

Fig. 7 Beam at the top of the lunettes and its mortise and tenon connections

Software: AutoCAD

Fig. 8 Damage observed in-situ in a representative bay: **a** failure of timber connections, **b** rocking motion of the pilasters

Fig. 9 Distribution of displacements in the model of the timber substructure under self-weight (m)

Software: Midas FX+ for DIANA

Fig. 10 Mode shapes with the participation mass percentage higher than 20%

Software: Midas FX+ for DIANA

Fig. 11 Comparison between the frequencies f and the mode shapes: **a** experimental results, **b** numerical results

Software: ARTeMIS and Midas FX+ for DIANA

Fig. 12 Comparison of the load-displacement diagrams obtained for the model of only the masonry envelope, calibrated (ME – C) and uncalibrated (ME – UC): **a** XX (or longitudinal) directions, **b** YY (or transversal) directions.

Software: Excel

Fig. 13 FE model of the whole structure in Midas FX+ for DIANA software

Software: Midas FX+ for DIANA

Fig. 14 Combined model under self-weight: **a** displacements (m), **b** minimum principal stresses (MPa), **c** crack widths (m)

Software: Midas FX+ for DIANA

Fig. 15 Combined model under lateral loading in the XX– direction: **a** displacements under 0.45g (m), **b** crack widths under 0.45g (m), **c** crack widths under 0.30g, after the peak (m)

Software: Midas FX+ for DIANA

Fig. 16 Combined model under lateral loading in the YY– direction: **a** displacements under 0.28g (m), **b** crack widths under 0.28g (m), **c** crack widths under 0.22g, after the peak (m)

Fig. 17 Comparison of the peak ground acceleration (PGA) with the load-displacement diagrams obtained for the combined model (MC) and for the calibrated model of only the masonry envelope

(ME – C): **a** XX– (longitudinal direction, top of the pediment), **b** YY– (transversal direction, top of the north-western corner)

Software: Excel

Fig. 18 Ground motions used for the nonlinear dynamic analysis: **a** comparison between the elastic response spectrum of the Peruvian Code and the artificial accelerograms, **b** artificial accelerograms generated for the two directions

Software: Excel

Fig. 19 Displacement-time diagrams obtained from nonlinear dynamic analysis

Software: Excel

Fig. 20 Correlation of cracks observed in the numerical model and in-situ: **a** detail of damage observed in-situ for the front façade [7], **b** tensile strains from nonlinear static analysis in the XX– direction, **c** tensile strains from nonlinear dynamic analysis

Software: Midas FX+ for DIANA

Fig. 21 Correlation of cracks observed in the numerical model and in-situ: **a** detail of damage observed in-situ for the northern lateral wall, **b** tensile strains from nonlinear static analysis in the YY– direction, **c** tensile strains from nonlinear dynamic analysis

Software: Midas FX+ for DIANA

Fig. 1 Ica Cathedral damage after the earthquakes in 2007 and 2009: **a** front façade, **b** main dome at transept, **c** barrel vaults with lunettes and pillars

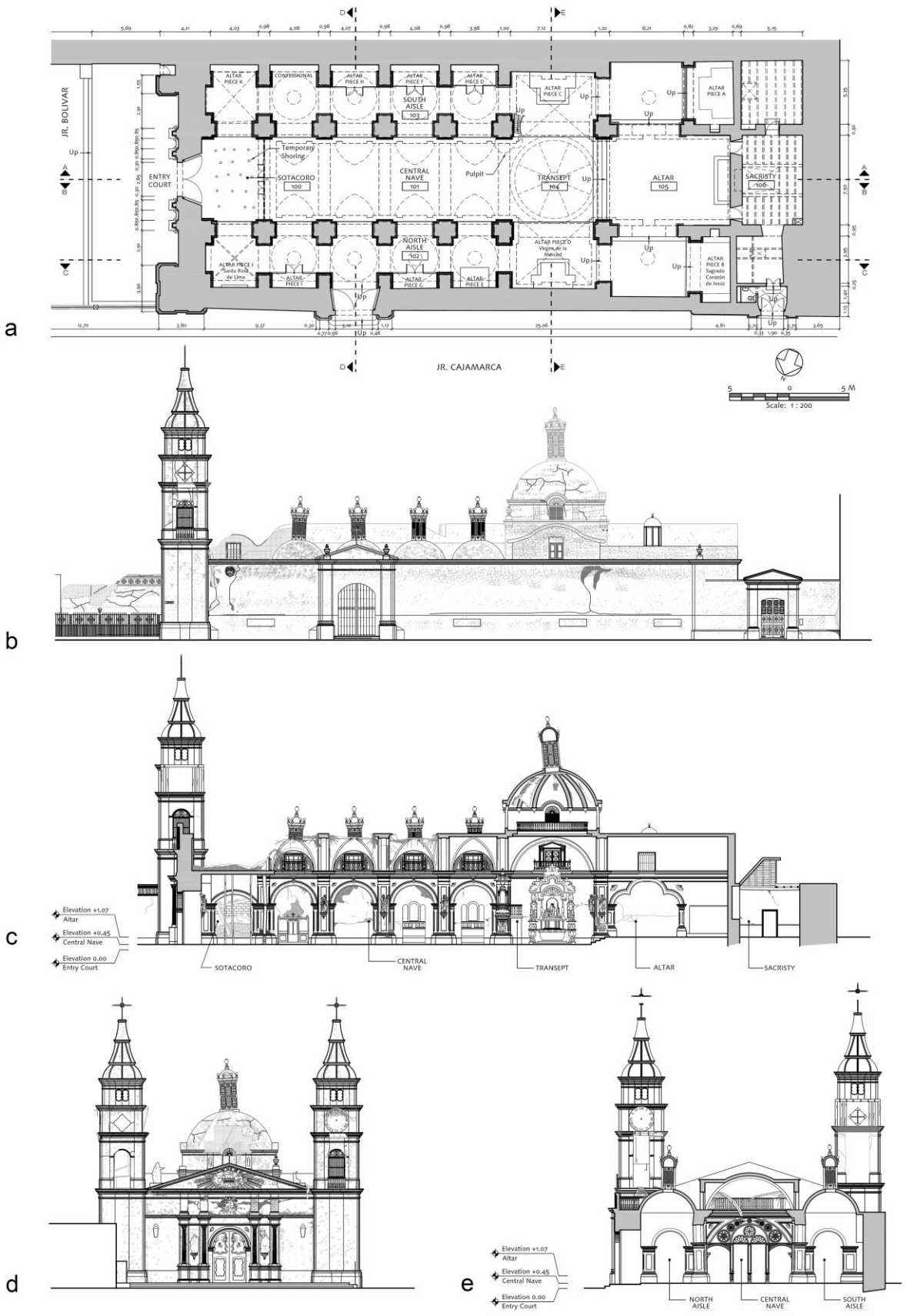

Fig. 2 Architectural drawing of Ica Cathedral: **a** ground floor, **b** longitudinal elevation, **c** longitudinal section, **d** front elevation, **e** transversal section (m) [7]

Fig. 3 Connection between the two substructures: **a** front façade/*sotacoro*, **b** piers along the lateral walls/timber beams

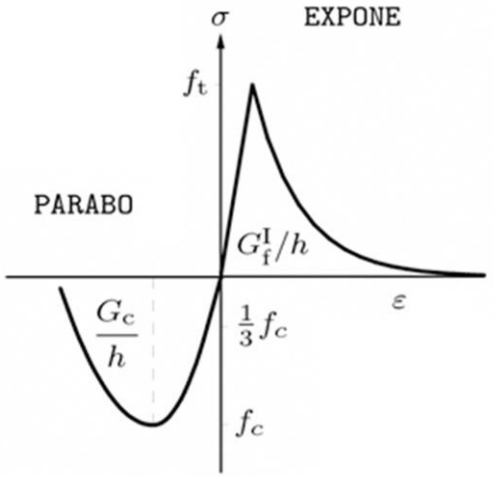

Fig. 4 Stress-strain curve showing the Total Strain Rotating Crack material model of masonry adopted in the numerical models [38]

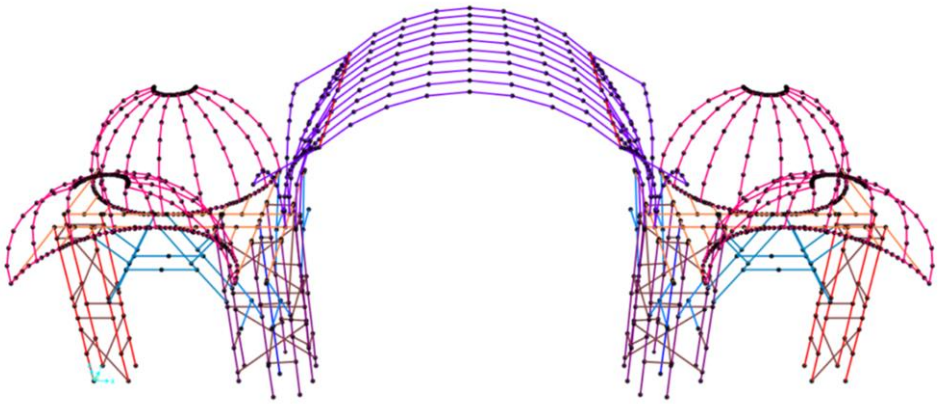

Fig. 5 FE model of the representative bay

Software: SAP 2000

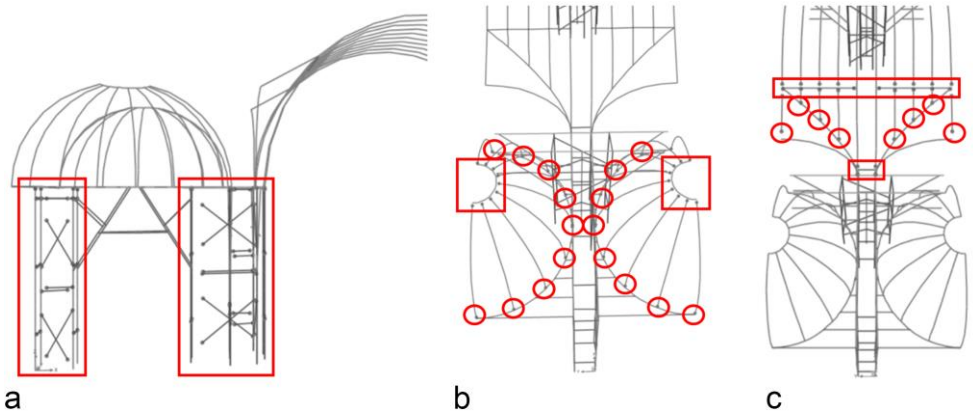

Fig. 6 Set of timber connections for parametric analyses considering hinged connections of elements: **a** model SB-1, **b** model SB-2, **c** model SB-3

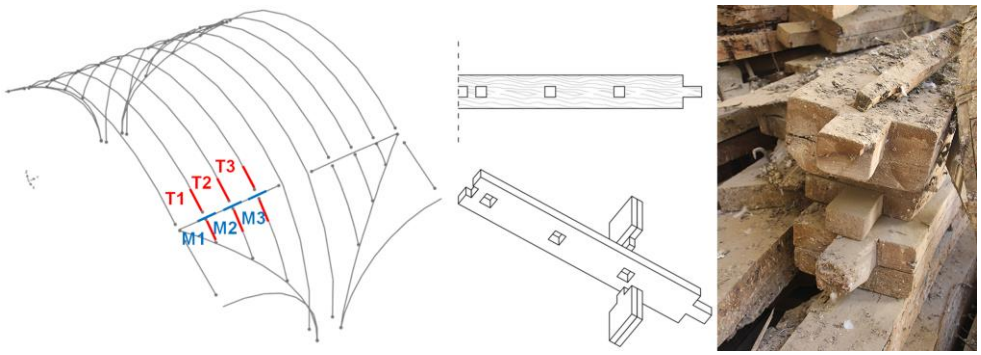

Fig. 7 Beam at the top of the lunettes and its mortise and tenon connections

Software: AutoCAD

a b

Fig. 8 Damage observed in-situ in a representative bay: **a** failure of timber connections, **b** rocking motion of the pilasters

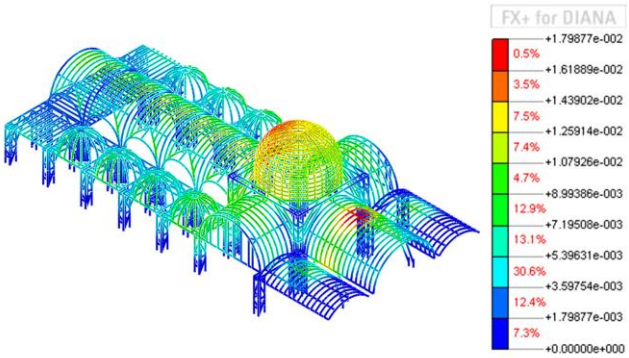

Fig. 9 Distribution of displacements in the model of the timber substructure under self-weight (m)

Software: Midas FX+ for DIANA

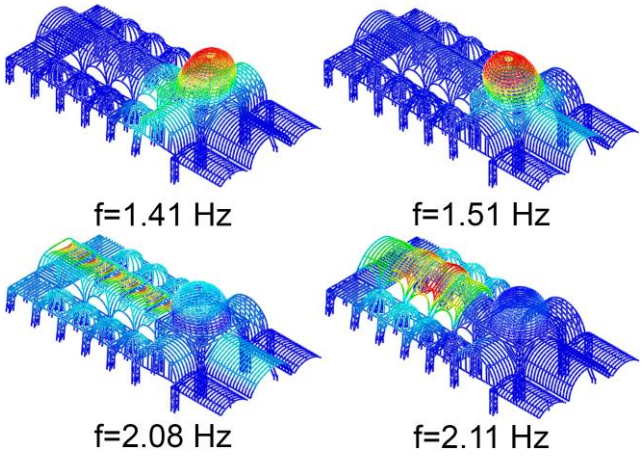

Fig. 10 Mode shapes with the participation mass percentage higher than 20%

Software: Midas FX+ for DIANA

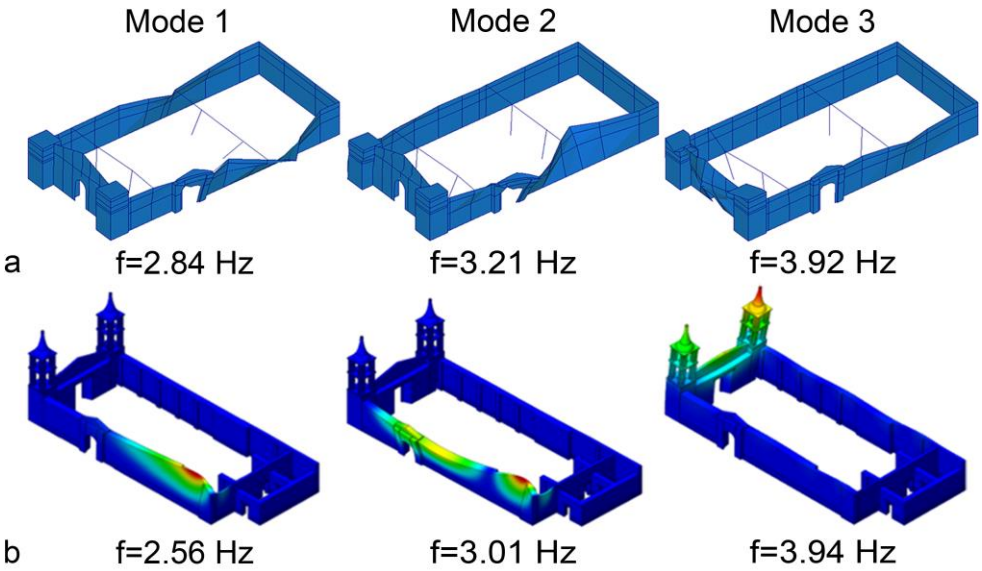

Fig. 11 Comparison between the frequencies f and the mode shapes: **a** experimental results, **b** numerical results

Software: ARTeMIS and Midas FX+ for DIANA

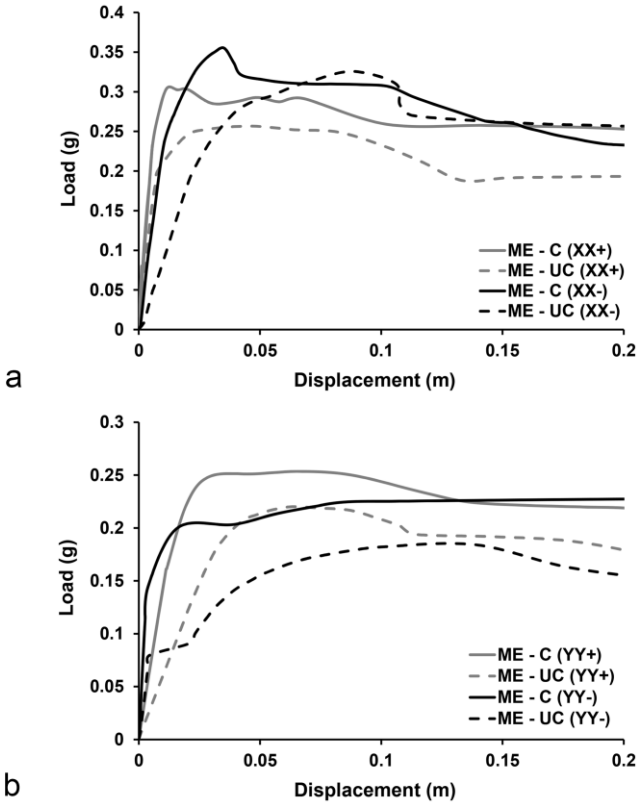

Fig. 12 Comparison of the load-displacement diagrams obtained for the model of only the masonry envelope, calibrated (ME – C) and uncalibrated (ME – UC): **a** XX (or longitudinal) directions, **b** YY (or transversal) directions.

Software: Excel

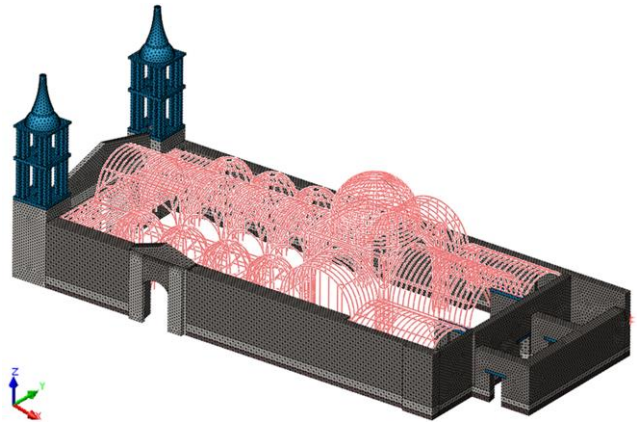

Fig. 13 FE model of the whole structure in Midas FX+ for DIANA software

Software: Midas FX+ for DIANA

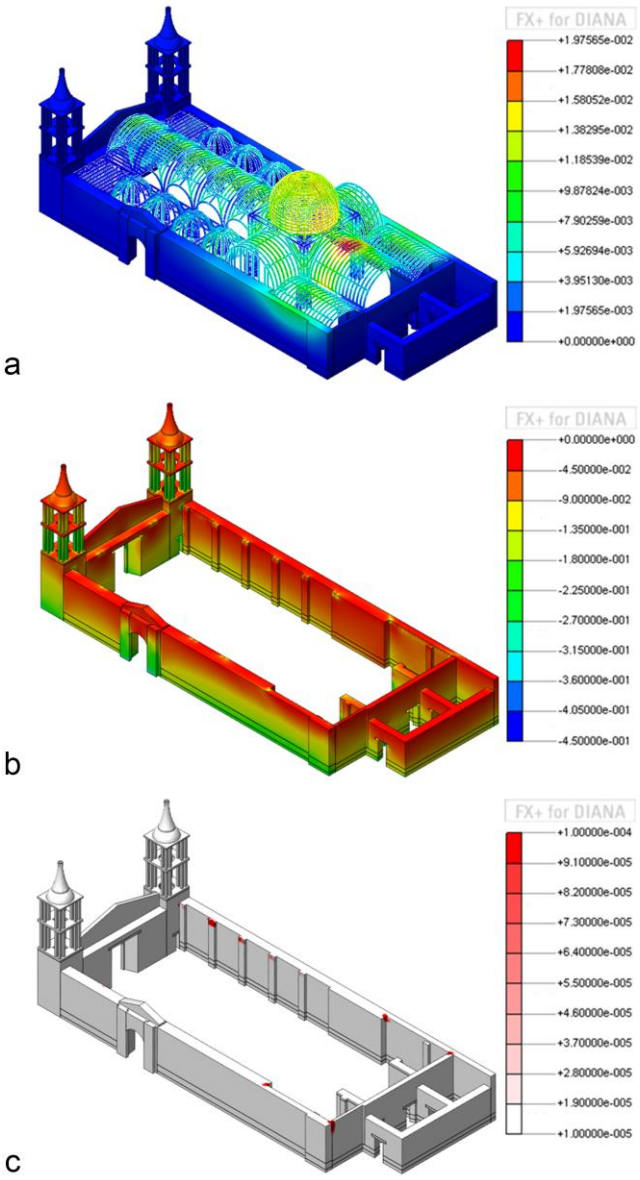

Fig. 14 Combined model under self-weight: **a** displacements (m), **b** minimum principal stresses (MPa), **c** crack widths (m)

Software: Midas FX+ for DIANA

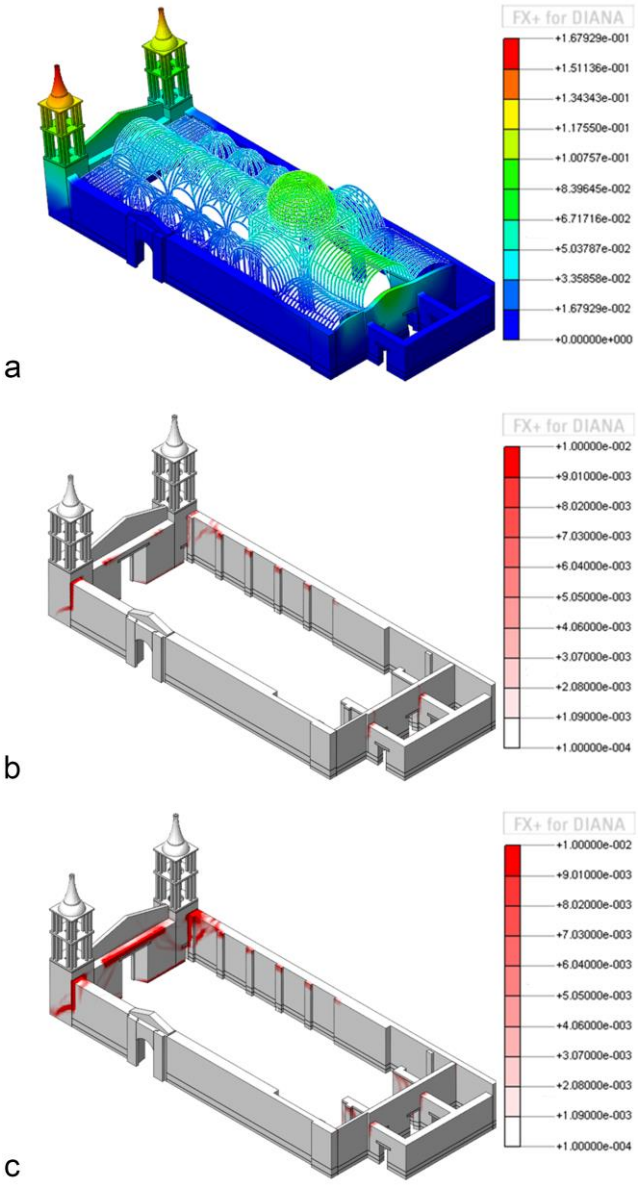

Fig. 15 Combined model under lateral loading in the XX– direction: **a** displacements under 0.45g (m), **b** crack widths under 0.45g (m), **c** crack widths under 0.30g, after the peak (m)

Software: Midas FX+ for DIANA

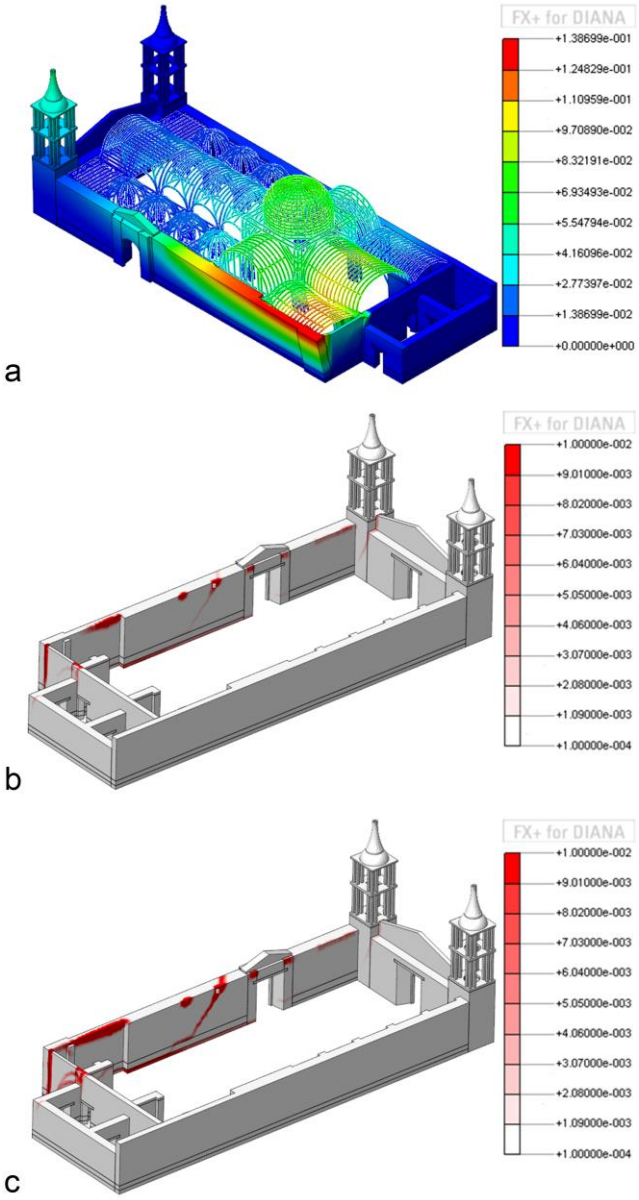

Fig. 16 Combined model under lateral loading in the YY– direction: **a** displacements under 0.28g (m), **b** crack widths under 0.28g (m), **c** crack widths under 0.22g, after the peak (m)

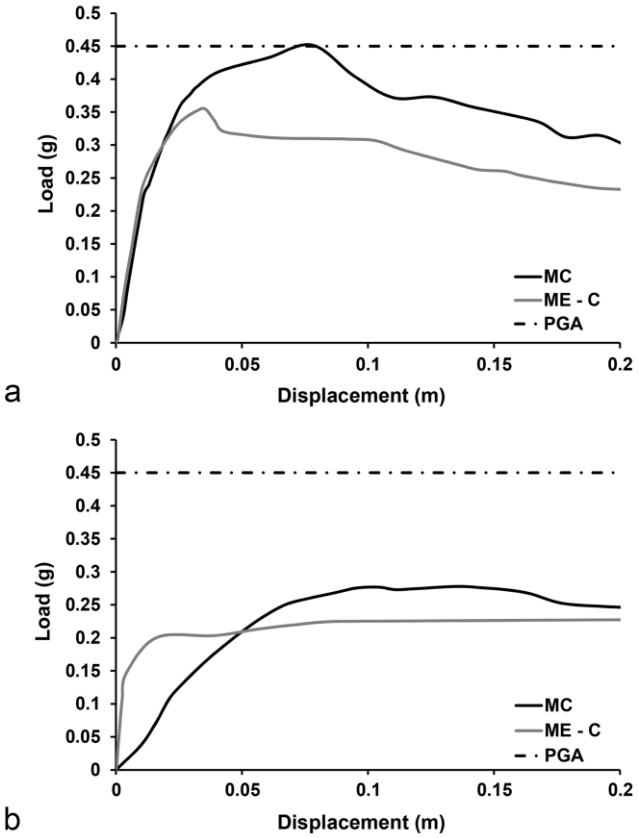

Fig. 17 Comparison of the peak ground acceleration (PGA) with the load-displacement diagrams obtained for the combined model (MC) and for the calibrated model of only the masonry envelope (ME – C): **a** XX– (longitudinal direction, top of the pediment), **b** YY– (transversal direction, top of the north-western corner)

Software: Excel

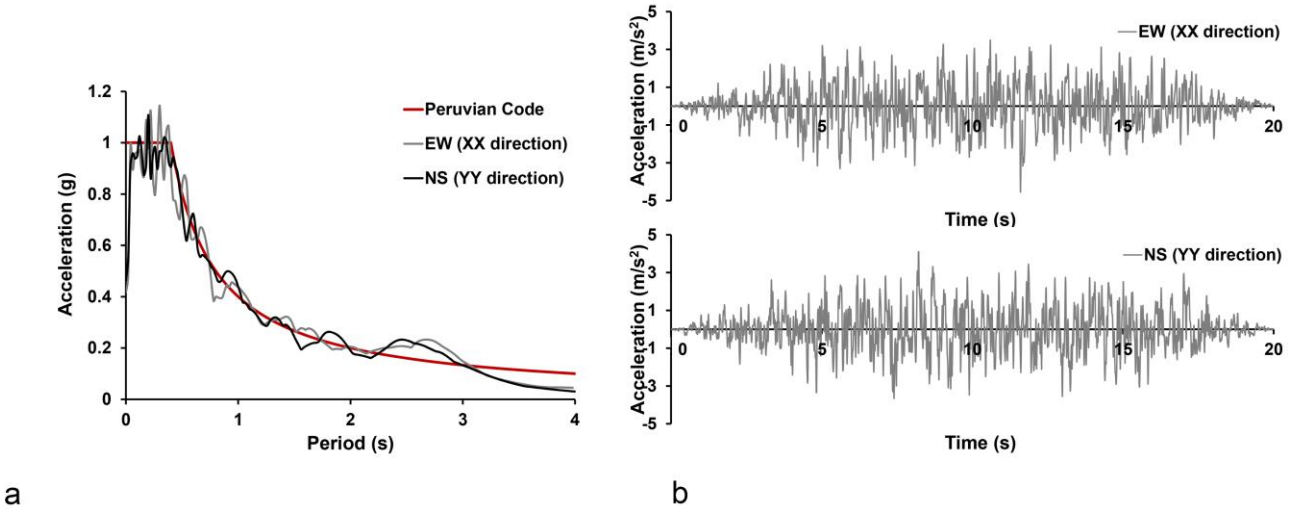

Fig. 18 Ground motions used for the nonlinear dynamic analysis: **a** comparison between the elastic response spectrum of the Peruvian Code and the artificial accelerograms, **b** artificial accelerograms generated for the two directions

Software: Excel

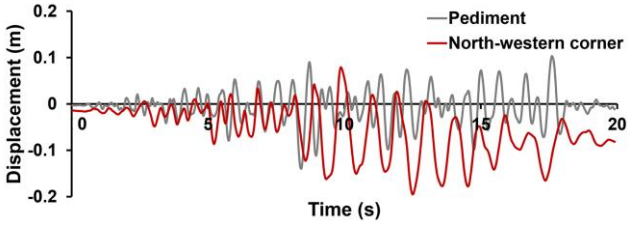

Fig. 19 Displacement-time diagrams obtained from nonlinear dynamic analysis

Software: Excel

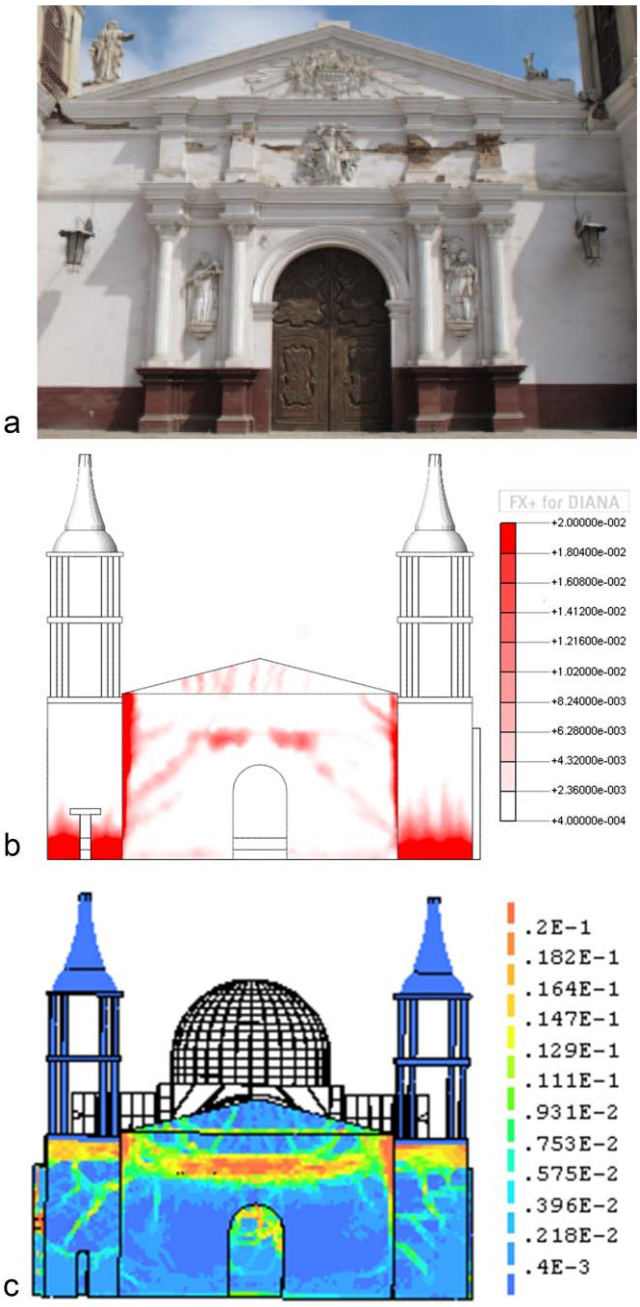

Fig. 20 Correlation of cracks observed in the numerical model and in-situ: **a** detail of damage observed in-situ for the front façade [7], **b** tensile strains from nonlinear static analysis in the XX–direction, **c** tensile strains from nonlinear dynamic analysis

Software: Midas FX+ for DIANA

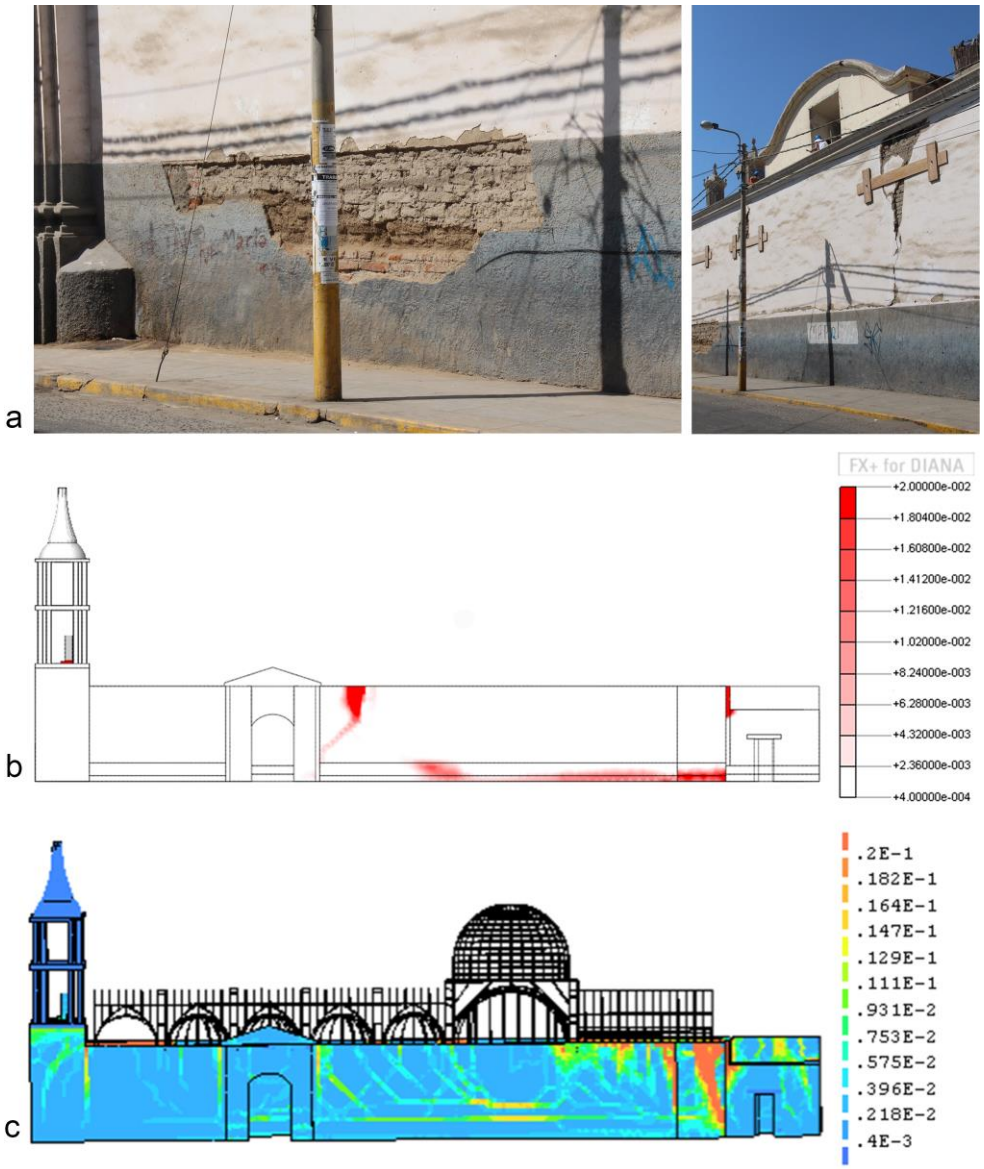

Fig. 21 Correlation of cracks observed in the numerical model and in-situ: **a** detail of damage observed in-situ for the northern lateral wall, **b** tensile strains from nonlinear static analysis in the YY– direction, **c** tensile strains from nonlinear dynamic analysis

Software: Midas FX+ for DIANA

View publication stats